Available online at www.sciencedirect.com
ScienceDirect
Surface & Coatings Technology 201 (2007) 5223 – 5227
SURFACE & COATINGS TECHNOLOGY
www.elsevier.com/locate/surfcoat

Microstructures, mechanical properties, and tribological behaviors of Cr–Al–N, Cr–Si–N, and Cr–Al–Si–N coatings by a hybrid coating system

In-Wook Park [a], Dong Shik Kang [b], John J. Moore [a], Sik Chol Kwon [c], Jong Joo Rha [c], Kwang Ho Kim [b,*]

[a] *Advanced Coatings and Surface Engineering Laboratory (ACSEL), Colorado School of Mines, 1500 Illinois Street, Golden, Colorado 80401, United States*
[b] *School of Materials Science and Engineering, Pusan National University, Busan 609-735, South Korea*
[c] *Korea Institute of Machinery and Materials (KIMM), Changwon, Kyungnam-do 641-010, South Korea*

Available online 22 August 2006

Abstract

Cr–Al–N, Cr–Si–N, Cr–Al–Si–N coatings were successfully deposited on WC–Co substrates by a hybrid coating system combining an arc ion plating technique using Cr target, and a magnetron sputtering method using Al and Si targets under N_2/Ar atmosphere. XRD, HRTEM, and XPS analyses revealed that the synthesized Cr–Al–N coatings consisted of solid-solution (Cr,Al)N crystallites, and the Cr–Si–N and Cr–Al–Si–N coatings with Si content of ~9 at.% were fine composites consisting of (Cr,Si)N and (Cr,Al,Si)N crystallites, respectively, embedded in an amorphous Si_3N_4/SiO_2 matrix. The hardness values of the Cr–Si–N (~35 GPa) and the Cr–Al–Si–N (~55 GPa) coatings were significantly increased compared with those of CrN (~23 GPa) and Cr–Al–N (~25 GPa) coatings. Besides, the average friction coefficients of the Cr–Si–N (~0.30) and the Cr–Al–Si–N (~0.57) coatings with Si content of about 9 at.% were largely decreased compared with those of CrN (~0.50) and Cr–Al–N (~0.84) coatings. A comparative study on microstructural characteristics among Cr–Al–N, Cr–Si–N, and Cr–Al–Si–N coatings is reported in this paper.

PACS: 46.55+d
Keywords: Cr–Al–N; Cr–Si–N; Cr–Al–Si–N; Mechanical properties; Tribological behaviors

1. Introduction

Chromium nitride (CrN) coatings have been widely used as protective coatings for various tribological forming and casting applications [1,2], because the coatings have high hardness as well as good wear-resistance due to its low friction coefficient. CrN coatings also show excellent corrosion-resistance under severe environmental condition [3] and good oxidation-resistance [4]. Recently, ternary Cr–X–N coatings, where X is the alloying element such as Ti [5,6], Al [7,8], Si [9,10], B [11], C [12,13], Ta [14,15], Nb [16], and Ni [17], etc., have been actively investigated to improve the properties of CrN coatings. Among these ternary systems, Cr–Al–N films have higher hardness (25–32 GPa) than that of CrN coatings, and have much improved oxidation-resistance up to 900 °C due to the formation of stable oxidation barrier of Al_2O_3 layer by migrated Al atoms to surface region [18,19]. Besides, Cr–Si–N coatings based on nanocomposite consisting of nanosized CrN crystallites and an amorphous SiN_x phase have been explored [20,21] to improve the hardness and tribological properties. More recently, quaternary Cr–Al–Si–N coatings start to be explored since it could become multi-functional coatings having superhardness (≥40 GPa), excellent oxidation- and wear-resistance. To our knowledge, no previous research was found in the literatures on the quaternary Cr–Al–Si–N coatings up to the present. For these reasons, we investigated the microstructure, mechanical properties, and tribological behaviors of quaternary Cr–Al–Si–N coatings compared with ternary Cr–Al–N and Cr–Si–N coatings.

In this work, Cr–Al–N, Cr–Si–N, and Cr–Al–Si–N coatings have been deposited on WC–Co substrates using the hybrid coating system of arc ion plating and magnetron sputtering

* Corresponding author. Tel.: +82 51 510 2391; fax: +82 51 510 3660.
E-mail address: kwhokim@pusan.ac.kr (K.H. Kim).

0257-8972/$ - see front matter © 2006 Elsevier B.V. All rights reserved.
doi:10.1016/j.surfcoat.2006.07.118

Table 1
Typical deposition conditions for CrN, Cr–Al–N, Cr–Si–N, and Cr–Al–Si–N coatings by the hybrid coating system

Variable		CrN	Cr–Al–N	Cr–Si–N	Cr–Al–Si–N
Arc	Cr target current	55 A	55 A	55 A	55 A
Sputter	Al target current	–	1.4 A	–	1.4 A
	Si target currents	–	–	0–2.2 A	0–2.2 A
N_2 : Ar ratio					2 : 1
Base pressure					2.7×10^{-3} Pa
Working pressure					4.0 Pa
Substrate temperature					300 °C
Substrate to target distance					300 mm
Substrate rotation speed					25 rpm
Typical coatings thickness					~2 μm

techniques. The relationship among microstructure, mechanical properties, and tribological behaviors of Cr–Al–N, Cr–Si–N, and Cr–Al–Si–N coatings was comparatively investigated.

2. Experimental

2.1. Deposition

The Cr–Al–N, Cr–Si–N, and Cr–Al–Si–N coatings were deposited on WC–Co and Si wafer substrates using the hybrid coating system, where the AIP method was combined with a magnetron sputtering technique. Arc cathode guns for Cr source and dc sputter gun for Al and Si sources were installed on each side of the chamber wall. A rotational substrate holder was located between the sources. Ar gas (99.999%) was introduced into the sputter target holder to increase the sputtering rate and N_2 gas (99.999%) was injected near the substrate holder. Purities of Cr, Al and Si targets were 99.99%. The WC–Co substrates of the disc type (20 mm in diameter and 3 mm in thickness) were cleaned in an ultrasonic cleaner using acetone and alcohol for 20 min. The substrates were cleaned again by ion bombardment using a bias voltage of −600 V under Ar atmosphere of 32 Pa for 15 min. The substrates were heated by resistant heaters set inside the chamber, and then the coatings were deposited from arc and sputter sources at a working pressure of 4 Pa. The deposition temperature was fixed at 300 °C. Typical deposition conditions for Cr–Al–N, Cr–Si–N, and Cr–Al–Si–N coatings by the hybrid coating system are summarized in Table 1.

Table 2
Chemical composition of the CrN, Cr–Al–N, Cr–Si–N and Cr–Al–Si–N coatings

	Elements		
	Cr (at.%)	Al (at.%)	N (at.%)
CrN	50	–	50±2
Cr–Al–N	33	17	50±2
Cr–Si(3 at.%)–N	47	–	50±2
Cr–Si(6.5 at.%)–N	43.5	–	50±2
Cr–Si(9.3 at.%)–N	40.7	–	50±2
Cr–Si(11 at.%)–N	39	–	50±2
Cr–Si(12.5 at.%)–N	37.5	–	50±2
Cr–Al–Si(4.5 at.%)–N	34	10.5	50±2
Cr–Al–Si(8.7 at.%)–N	31.7	9.2	50±2
Cr–Al–Si(9.8 at.%)–N	30.2	9	50±2
Cr–Al–Si(12.4 at.%)–N	29	8.8	50±2
Cr–Al–Si(16 at.%)–N	26.5	7	50±2

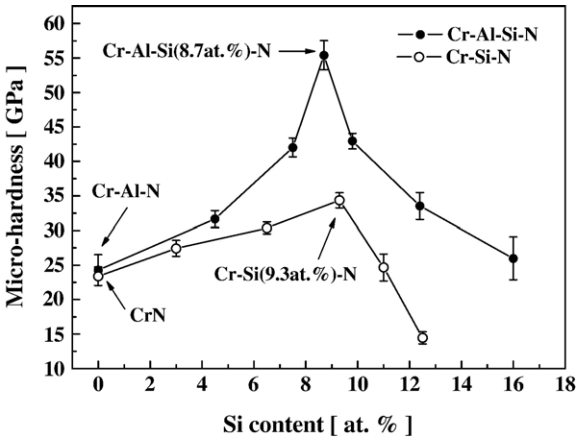

Fig. 1. Microhardness of the Cr–Si–N and Cr–Al–Si–N coatings as a function of Si content.

2.2. Characterization

The coating thickness was measured using a scanning electron microscopy (SEM, Hitachi, S-4200) and a stylus (α-STEP) instrument. Compositional analyses of the coatings to determine the contents of Cr, Al, Si and N were carried out by electron probe microanalyzer (EPMA, Shimadzu, EPMA 1600). Chemical compostions of the various coatings are shown in Table 2. The crystallinity of the Cr–Al–Si–N coatings was analyzed with X-ray diffractometer (XRD, PHILIPS, X'Pert-MPD System) using CuKα radiation. X-ray photoelectron spectroscopy (XPS, VG Scientifics, ESCALAB 250) was also performed to study the bonding status in the Cr–Si–N and Cr–Al–Si–N coatings. The XPS spectra were obtained after removing the surface layer of samples by sputtering with Ar^+ ions (3 keV) for 3 min and the spectra were calibrated for the value of carbon peak C 1s at

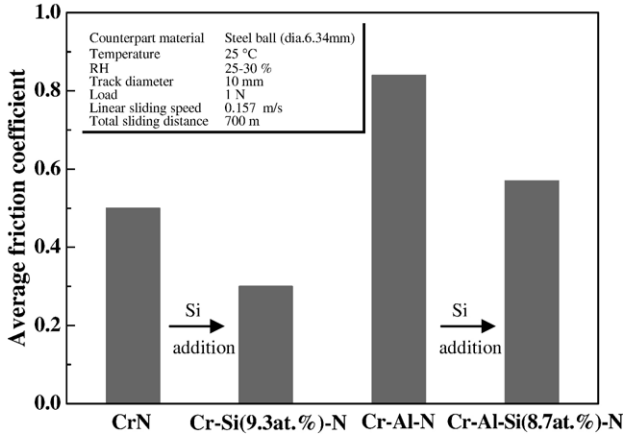

Fig. 2. Average friction coefficients of CrN, Cr–Si(9.3 at.%)–N, Cr–Al–N, and Cr–Al–Si(8.7 at.%)–N coatings against steel ball.

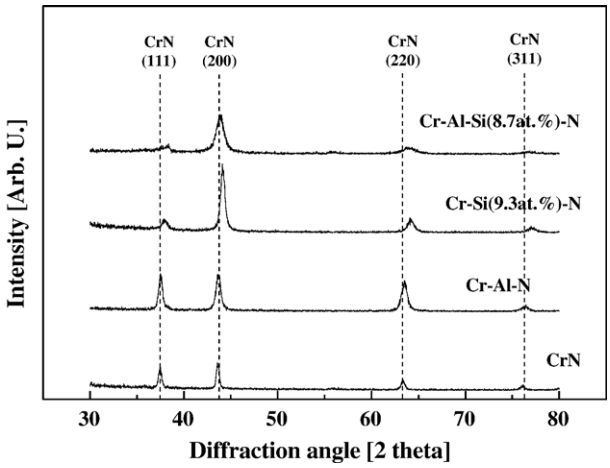

Fig. 3. X-ray diffraction patterns of CrN, Cr–Al–N, Cr–Si(9.3 at.%)–N, and Cr–Al–Si(8.7 at.%)–N coatings.

284.5 eV. Structural information on the coatings was obtained from the high-resolution transmission electron microscopy (HRTEM) using a field emission transmission electron microscope (FE-TEM, JEOL, JEM-2012F) with a 200 kV acceleration voltage. The hardness of coatings was evaluated using a microhardness tester with Knoop indenter (Matsuzawa, MMT-7) under a load of 25 g. The friction coefficient and wear behaviors were evaluated through sliding tests using a conventional ball-on-disc wear apparatus. A steel ball (diameter 6.34 mm, 700 $Hv_{0.2}$) was used as a counterpart material. The sliding tests were conducted with a sliding speed of 0.157 m/s under a load of 1 N at ambient temperature (around 25 °C) and relative humidity (25–30% RH) condition. Scanning electron microscopy was employed to observe the morphology of the wear track after each sliding experiment. Energy dispersive spectroscopy (EDS) was used to reveal the compositions of wear debris formed during the wear experiment.

3. Results and discussion

Fig. 1 shows the microhardness of the Cr–Si–N and Cr–Al–Si–N coatings as a function of Si content. As the Si content increased in the coatings, the hardness of the Cr–Si–N coatings gradually increased from ~23 GPa for CrN, reached maximum hardness value of ~35 GPa at the Si content of around 9.3 at.%. Also, the hardness of the Cr–Al–Si–N coatings steeply increased from ~25 GPa for Cr–Al–N coatings with Al content of 17 at.%, and showed maximum value of ~55 GPa at the Si content of 8.7 at.%. However, the hardness of Cr–Si–N and Cr–Al–Si–N coatings reduced with further increase in the Si content. Fig. 2 illustrates the average friction coefficients of CrN, Cr–Al–N, Cr–Si(9.3 at.%)–N, and Cr–Al–Si(8.7 at.%)–N coatings against steel ball. The average friction coefficients of the Cr–Si(9.3 at.%)–N and Cr–Al–Si(8.7 at.%)–N coatings were largely decreased from 0.51 for CrN coatings and 0.84 for Cr–Al–N coatings to 0.30 and 0.57, respectively, with Si addition of around 9 at.%.

Fig. 3 shows the X-ray diffraction patterns of CrN, Cr–Al–N, Cr–Si(9.3 at.%)–N, and Cr–Al–Si(8.7 at.%)–N coatings. The diffraction pattern of CrN coatings showed the B1 NaCl crystal type of CrN crystalline with multiple orientations of (111), (200), (220), and (311). As the element Al or Si was incorporated into CrN, the diffraction peak position was a little shifted to higher angle compared to pure CrN crystals. These peak shift phenomena reflect that the added Al and Si would be dissolved into CrN lattice by substitutional replacement of smaller Si atoms for Cr sites. However, the diffraction peak intensities reduced and the peak shape were broadened in case of Cr–Al–Si(8.7 at.%)–N coatings compared to Cr–Al–N coatings. Such an XRD peak broadening, in general, is an indication of either diminution of the grain size or non-uniform residual stress in the crystal lattice in the coating [22]. Any XRD peaks corresponding to Cr_2N, Cr, Si_3N_4, $CrSi_2$, and AlN were not observed in Fig. 3. Fig. 4 shows the cross-sectional HRTEM images and their electron diffraction patterns for Cr–Al–N, Cr–Si(9.3 at.%)–N, and Cr–Al–Si(8.7 at.%)–N coatings. In Fig. 4 (a), HRTEM image and diffraction pattern indicate that the Cr–

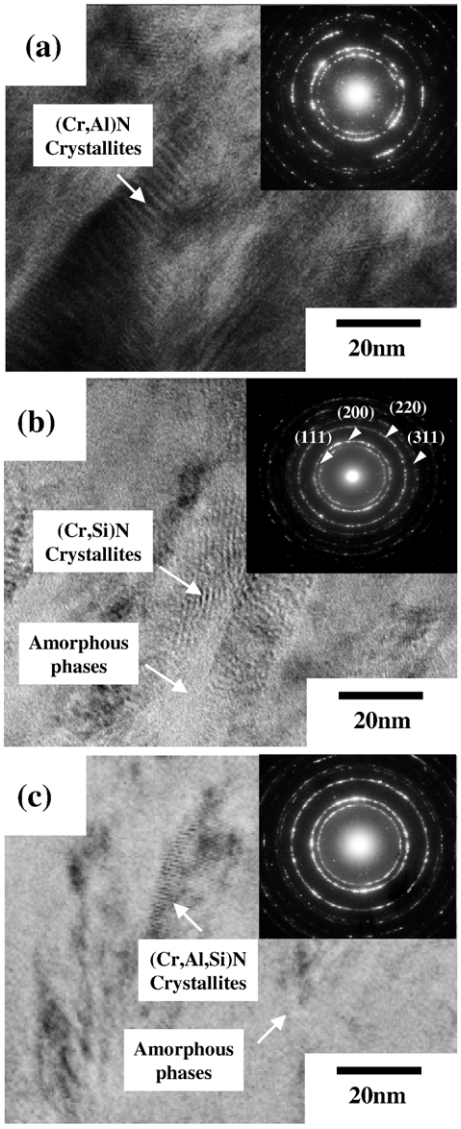

Fig. 4. Cross-sectional HRTEM images and their electron diffraction patterns for (a) Cr–Al–N, (b) Cr–Si(9.3 at.%)–N, and (c) Cr–Al–Si(8.7 at.%)–N coatings.

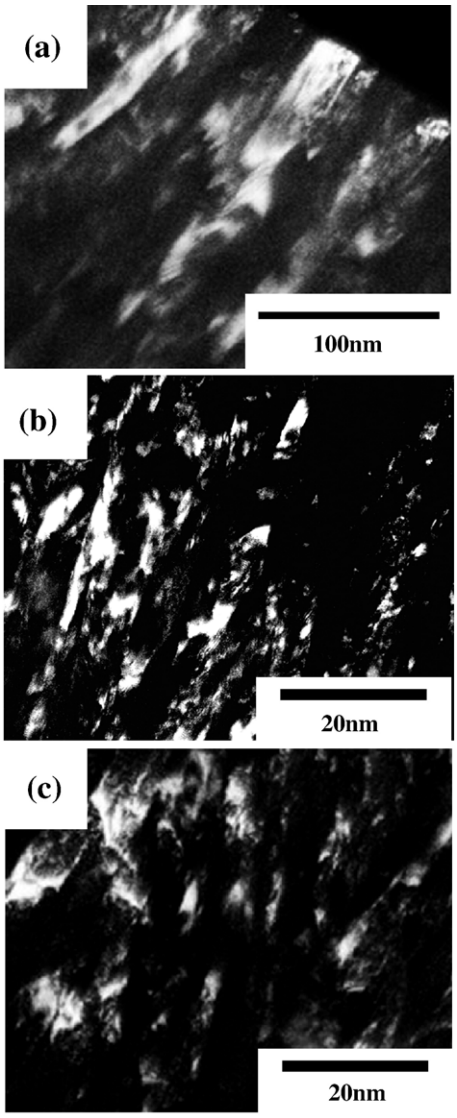

Fig. 5. Dark-field TEM images of (a) Cr–Al–N, (b) Cr–Si(9.3 at.%)–N, and (c) Cr–Al–Si(8.7 at.%)–N coatings.

Al–N coatings was composed of relatively large grains. On the other hand, the Cr–Si–N and Cr–Al–Si–N coatings were found from Fig. 4(b) and (c) to be composites consisted of fine crystallites and amorphous phase. These crystallites could be distinguished from each other by lattice fringe contrast. The crystallites had irregular and ellipsoidal shapes with size ranging from 15 to 25 nm, and were not fully homogeneously distributed in the amorphous phase. Fig. 5 shows the dark-field TEM images of Cr–Al–N, Cr–Si(9.3 at.%)–N, and Cr–Al–Si (8.7 at.%)–N coatings. It was found from Fig. 5 that the Cr–Al–Si(8.7 at.%)–N coatings as well as Cr–Si(9.3 at.%)–N were composed of much finer crystallites of CrN and Cr–Al–N, respectively, while the Cr–Al–N coatings had a microstructure of large grains with columnar structure. This microstructural change with Si incorporation into Cr–Al–N is similar to the case of the Si addition into Ti–Al–N, as previously reported by the authors for the nc-(Ti,Al,Si)N/a-Si_3N_4 nanocomposite system [23]. The microstructural evolution with Si addition into Cr–Al–N coatings can be also explained with the percolation phenomenon of amorphous phase into Cr–Al–N crystalline phase.

In order to investigate the bonding status of Si in the coatings, XPS was performed on Cr–Si–N and Cr–Al–Si–N coatings. Fig. 6 shows the XPS spectra near binding energies of Si for the Cr–Si(9.3 at.%)–N and Cr–Al–Si(8.7 at.%)–N coatings. The binding energies of Si 2p for both coatings appeared at 101.8 eV, which are in good agreement with those of stoichiometric Si_3N_4 [24]. In addition, little peaks corresponding to SiO_2 phase and free silicon also appeared at 103.0 eV and 99.4 eV, respectively [24]. Kim et al. [25] found that the free Si could appear due to the deficit of the nitrogen source during the sputtering process at the high Si content of Ti–Si–N coatings, and verified that the free Si disappeared by sufficient nitrogen supply during deposition. Small amount of SiO_2 phase was found to be incorporated into the coatings. The oxygen source seems to be derived from the target or chamber.

Based on the results from our XRD, HRTEM, and XPS analyses, it was concluded that the Cr–Si–N and Cr–Al–Si–N coatings were nanocomposites consisting of nanosized (Cr,Si)N and (Cr,Al,Si)N crystallites embedded in amorphous Si_3N_4 and SiO_2 matrix, respectively while Cr–Al–N coatings consisted of solid-solution (Cr,Al)N crystallites only.

The hardness of the Cr–Si–N and Cr–Al–Si–N coatings showed the maximum values at a Si content of around 9 at.% in Fig. 1. The maximum hardness values of the Cr–Si–N (~35 GPa) and Cr–Al–Si–N (~55 GPa) coatings were significantly increased compared with those of CrN (~23 GPa) and Cr–Al–N (~25 GPa) coatings. The large increase in the hardness value for Cr–Si–N and Cr–Al–Si–N coatings with about 9 at.% Si addition can be explained with a grain boundary hardening phenomena created by strong cohesive energy of interphase boundaries [26] and by the Hall–Petch relation derived from crystal size refinement [27]. Both the formation of strong interphase boundaries and the refinement of crystallites resulted from the percolation phenomenon of amorphous Si_3N_4 and SiO_2 phases into the CrN and Cr–Al–N coatings, respectively. Another

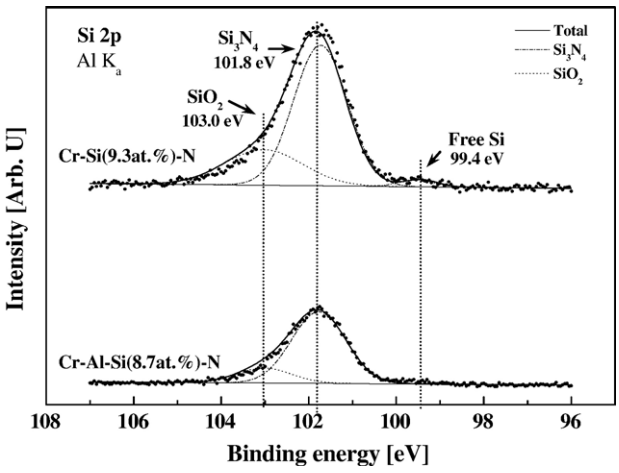

Fig. 6. XPS spectra near binding energies of Si for Cr–Si(9.3 at.%)–N and Cr–Al–Si(8.7 at.%)–N coatings.

possible mechanism would be due to the solid-solution hardening of crystallites by Si dissolution into CrN and Cr–Al–N. On the other hand, the hardness reduction of Cr–Si–N and Cr–Al–Si–N coatings with the further increase of Si content above 10 at.% was suggested to be due to the increase of volume fraction of amorphous phase [28,29]. When the amorphous phase became thicker than crystallites, the hardness of coatings became strongly dependent on the property of the amorphous phase [25,28].

The average friction coefficients of the Cr–Si–N and Cr–Al–Si–N coatings were largely decreased by Si addition of ~9 at.%. This result would be caused by smoother surface [30] due to the existence of amorphous Si_3N_4 and SiO_2 phases in the Cr–Si(9.3 at.%)–N and Cr–Al–Si(8.7 at.%)–N coatings, and would be also caused by following tribochemical reactions between Si and ambient humidity [31].

$$Si_3N_4 + 6H_2O = 3SiO_2 + 4NH_3$$

$$SiO_2 + H_2O = Si(OH)_4$$

These products of SiO_2 and $Si(OH)_2$ were known to play a role as a self-lubricating layer [32]. The formation of tribo-layer would be more activated with increasing Si content in the Cr–Si (9.3 at.%)–N and Cr–Al–Si(8.7 at.%)–N coatings.

4. Conclusions

Cr–Al–N, Cr–Si–N, and Cr–Al–Si–N coatings were deposited on WC–Co substrates using a hybrid coating system, in which AIP method was combined with a magnetron sputtering technique. The instrumental analyses revealed that the synthesized Cr–Al–N coatings consisted of solid-solution (Cr,Al)N crystallites, and the Cr–Si–N and Cr–Al–Si–N coatings with Si content of around 9 at.% were nanocomposites consisting of nanosized (Cr,Si)N or (Cr,Al,Si)N crystallites embedded in an amorphous Si_3N_4/SiO_2 matrix. The hardness of the Cr–Si–N and Cr–Al–Si–N coatings exhibited the maximum hardness values of ~35 GPa and ~55 GPa, respectively, at a Si content of ~9 at.% due to the microstructural change to a nanocomposite as well as the solid-solution hardening. The average friction coefficients of the Cr–Si–N and the Cr–Al–Si–N coatings with Si content of about 9 at.% were largely decreased compared with those of CrN and Cr–Al–N coatings. The decrease of friction coefficient could be explained by tribochemical reaction between Si and ambient humidity as well as smoother surface due to amorphous phase.

Acknowledgments

This work was supported by a grant from the National Core Research Center (NCRC) Program (R15-2006-022-01002-0) funded by KOSEF and MOST.

References

[1] C. Rebholz, H. Ziegele, A. Leyland, A. Mattew, Surf. Coat. Technol. 115 (1999) 222.
[2] J. Creus, H. Indriss, H. Mazille, F. Sanchette, P. Jacquot, Surf. Coat. Technol. 107 (1998) 183.
[3] B. Navinsek, P. Panjan, I. Milosev, Surf. Coat. Technol. 97 (1997) 182.
[4] B. Navinsek, P. Panjan, Surf. Coat. Technol. 74–75 (1995) 919.
[5] X.T. Zeng, J. Vac. Sci. Technol., A, Vac. Surf. Films 17 (1999) 1991.
[6] J.J. Nainaparampil, J.S. Zabinski, A. Korenyi-Both, Thin Solid Films 333 (1998) 88.
[7] S. Ulrich, S. Sattel, Thin Solid Films 437 (2003) 164.
[8] J.C. Sánchez-López, D. Martínez-Martínez, C. López-Cartes, A. Fernández, M. Brizuela, A. García-Luis, J.I. Oñate, J. Vac. Sci. Technol., A, Vac. Surf. Films 23 (2005) 681.
[9] J.H. Park, W.S. Chung, Y.-R. Cho, K.H. Kim, Surf. Coat. Technol. 188 (2004) 425.
[10] E. Martinez, R. Sanjines, A. Karimi, J. Esteve, F. Lévy, Surf. Coat. Technol. 180 (2004) 570.
[11] B. Rother, H. Kappl, Surf. Coat. Technol. 96 (1997) 163.
[12] J. Almer, M. Oden, G. Hakansson, Thin Solid Films 385 (2001) 190.
[13] S.H. Yao, Y.L. Su, Wear 212 (1997) 85.
[14] M. Cekada, P. Panjan, B. Navinsek, F. Cvelbar, Vacuum 52 (1999) 461.
[15] R. Saha, R.B. Inturi, J.A. Barnard, Surf. Coat. Technol. 82 (1996) 42.
[16] J.N. Tan, J.H. Hsieh, Surf. Coat. Technol. 167 (2003) 154.
[17] F. Regent, J. Musil, Surf. Coat. Technol. 142 (2001) 146.
[18] M. Kawate, A.K. Hashimoto, T. Suzuki, Surf. Coat. Technol. 165 (2003) 163.
[19] O. Banakh, P.E. Schmid, R. Sanjines, F. Lévy, Surf. Coat. Technol. 163–164 (2003) 57.
[20] E. Martinez, R. Sanjines, F. Lévy, Surf. Coat. Technol. in press.
[21] D. Mercs, N. Bonasso, S. Naamane, J.-M. Bordes, C. Coddet, Surf. Coat. Technol. in press.
[22] M. Diserens, J. Patscheider, F. Lévy, Surf. Coat. Technol. 108–109 (1998) 241.
[23] I.-W. Park, S.R. Choi, M.-H. Lee, K.H. Kim, J. Vac. Sci. Technol., A, Vac. Surf. Films 21 (4) (2003) 895.
[24] J.F. Moulder, W.F. Stickle, P.E. Sobol, K.D. Bomben, Handbook of X-ray Photoelectron Spectroscopy, Physical Electronics, Inc, Minnesota, 1995, p. 238.
[25] S.H. Kim, J.K. Kim, K.H. Kim, Thin Solid Films 420–421 (2002) 360.
[26] S. Veprek, S. Reiprich, L. Shizhi, Appl. Phys. Lett. 66 (20) (1995) 2640.
[27] A. Lasalmonie, J.L. Strudel, J. Mater. Sci. 21 (1986) 1837.
[28] S. Vepřek, S. Reiprich, Thin Solid Films 268 (1995) 64.
[29] K.H. Kim, S.-R. Choi, S.-Y. Yoon, Surf. Coat. Technol. 161 (2002) 243.
[30] J. Takadoum, H. Houmid-Bennani, D. Mairey, J. Eur. Ceram. Soc. 18 (1998) 553.
[31] J. Xu, K. Kato, Wear 245 (2000) 61.
[32] S. Wilson, A.T. Alpas, Wear 245 (1996) 223.